Spatial Expression of Long Non-Coding RNAs in Human Brains of Alzheimer's Disease

Bernard Ng[1, #], Denis R. Avey[1, 5, #], Katia de Paiva Lopes[1], Masashi Fujita[2], Shinya Tasaki[1], Ricardo A. Vialle[1], Artemis Iatrou[1,3], Sashini De Tissera[1], Tien-Hao Chang[1], Jishu Xu[1], Himanshu Vyas[1], Nicola A. Kearns[1, 5], Vilas Menon[2], Chris Gaiteri[1,4], Philip L. De Jager[2], David A. Bennett[1, 5], Yanling Wang[1, 5, *]

1. Rush Alzheimer's Disease Center, Rush University Medical Center, Chicago, IL, 60612, USA
2. Center for Translational and Computational Neuroimmunology, Department of Neurology, Columbia University Irving Medical Center, New York, NY, USA
3. Current affiliation: Department of Psychiatry, McLean Hospital, Harvard Medical School, Belmont, MA, 02478, USA
4. Department of Psychiatry, Upstate Medical University, Syracuse, NY, 13210, USA
5. Department of Neurological Sciences, Rush University Medical Center, Chicago, IL, 60612, USA

[#]Contributed equally

*Correspondence to yanling_wang@rush.edu

Abstract

Long non-coding RNAs (lncRNAs) are highly versatile in their modes of action and play critical roles in both normal physiological and disease processes. The dysregulation of lncRNA expression has been implicated in aging and many neurological disorders, including Alzheimer's disease (AD). Here, we report a spatial expression atlas of 7,634 lncRNA genes in aged human brains, covering 258,987 microdomains from 78 postmortem brain sections of 21 ROSMAP participants. We detected a greater proportion of lncRNAs expressed specifically in distinct cortical subregions than mRNAs, and most belong to antisense and lincRNA biotypes. We generated 193 gene modules from gene networks of 8 subregions and identified lncRNA-enriched gene modules implicated in multiple AD-relevant biological processes. By cross-referencing published snRNA-seq data, we detected a partially overlapping but independent pattern between sub-region and cell-type specificity of lncRNA expression. We mapped spatially differentially expressed (SDE) lncRNAs and mRNAs in AD brains and observed that SDE lncRNAs encompass more subregion-specific transcripts. Gene set enrichment analysis indicates that AD SDE lncRNAs are involved in epigenetic regulation, chromatin remodeling, RNA metabolism, synaptic signaling, and apoptosis. Particularly relevant to AD therapeutic potentials is an enrichment for HDAC target genes, including *OIP5-AS1*, a lncRNA extensively studied in cancer and, most recently,

in AD. We then applied multivariate fine-mapping to the expression quantitative trait loci (eQTLs) proximal to the *OIP5-AS1* loci and identified rs1655558 as a potential genetic driver of *OIP5-AS1* expression. Using statistical modeling, we inferred that the interaction between *OIP5-AS1* and HDAC proteins, especially HDAC11, is associated with tau tangles in excitatory neurons and plaque burden in microglia. Our study represents a valuable resource of lncRNA spatial expression in the aged human brain, shedding mechanistic insights into their functional roles in AD and neurodegeneration.

Introduction

One remarkable yet unexpected discovery of the eukaryotic transcriptome in the 21st century is that a large portion of the genome is actively transcribed into RNAs with little or no protein-coding potential[1,2]. Specifically, about 90% of the human genome is transcribed, but only about 2% is annotated as protein-coding genes. Since this discovery, there has been a surge of publications highlighting the regulatory roles of non-coding RNAs (ncRNAs) in controlling gene expression[2,3], debunking the long-held belief that functional genetic information is only contained in protein-coding genes and RNAs are mere intermediaries along the central dogma between DNA and proteins.

Long non-coding RNAs (lncRNAs) belong to a class of ncRNAs that are longer than 200 nucleotides and are generated mainly by Polymerase II, with little or no protein-coding potential[4,5]. Accumulated studies show that lncRNAs affect gene expression through various regulatory mechanisms, including epigenetic modification, chromatin modeling, and post-transcriptional and translational regulations. Compared with coding RNAs, lncRNAs exhibit substantially greater tissue- and cell-type-specificity[6,7]. Notably, the number of lncRNAs often increases with the complexity of organisms. In the human genome, approximately 40% of lncRNAs are explicitly expressed in the brain, and many of those lncRNAs are involved in various biological processes, including neuronal differentiation, synaptogenesis, and neuroplasticity[1,8].

The dysregulation of lncRNA expression has been implicated in many neurological disorders, including brain aging and Alzheimer's disease (AD). In AD, aberrant expression of lncRNAs has been found in the brains of AD animal models and AD patients. Those dysregulated lncRNAs have been implicated in various aspects of AD pathogenesis, such as amyloid-beta metabolism, tau protein pathology, neuron inflammation, and cell death[9–13]. Despite these insights, our understanding of the spatial expression patterns of lncRNAs in the human brain remains limited, hindering our understanding of their functional roles in health and disease contexts.

Here, we report a spatial expression atlas of 7,634 lncRNA genes in aged human brains, covering 258,987 microdomains from 78 brain sections across 21 ROSMAP participants with and without AD

66 dementia. We identify spatially resolved lncRNA genes and lncRNA-enriched gene modules. We cross-
67 reference ROSMAP snRNA-seq data[14] to explore the patterns between sub-region and cell-type
68 specificity of lncRNA expression. We map spatially differentially expressed (SDE) lncRNAs and mRNAs
69 in AD brains and compare our ST findings with those from bulk RNA-seq and snRNA-seq. Finally, we
70 infer the potential functions of SDE lncRNAs and uncover a potential interaction between *OIP5-AS1*
71 and HDACs in mediating AD pathogenesis. Our study represents a valuable resource of lncRNA spatial
72 expression in the aged human brain, shedding mechanistic insights into their functional roles in AD and
73 neurodegeneration.

74 **Results**

75 **Spatial expression of lncRNAs in aged human brains**

76 Leveraging our recently acquired spatial transcriptomic data[15], we analyzed lncRNA expression in the
77 dorsolateral prefrontal cortex (DLPFC) from 78 brain sections across 21 female individuals (AD=13;
78 NCI=8). In total, we detected 7,634 lncRNAs and 16,769 protein-coding mRNAs across all spot clusters,
79 including Layer (L)1, L2-3, L3-5, L5, and L6, white matter (WM), meninges, and blood vessels (Fig 1A).
80 As expected, most lncRNAs present lower expressions than mRNAs (Fig. 1B). Out of the total ~260K
81 spots, we only detected lncRNAs in <0.01% of spots (Fig. 1C), and those lncRNAs are mostly long
82 intergenic non-coding RNAs (lincRNA) or antisense (Fig. 1D). We then assessed the subregion-
83 specificity of lncRNAs. We found a greater proportion of lncRNAs expressed in a single subregion (or
84 distinct subsets of subregions) than mRNAs (Fig. 1E).
85
86 Contrasting the expression of ST spots in one subregion against all other subregions, we identified 79
87 subregion-specific lncRNAs (Fig. 2A-B, Table S1). To examine whether subregion-specific lncRNA
88 aligns with cell-type-specific expression and vice versa, we cross-referenced a published snRNA-seq
89 dataset derived from the DLPFC of 424 ROSMAP individuals[14]. We found a subset of cell-type specific
90 lncRNAs (Table S1) aligns with the ST subregion-specific lncRNAs (Fig. 2C; Table S1). For example,
91 LINC00844 is highly expressed in WM (Fig 2A-B) and oligodendrocytes (Fig. 2C-D). In general,
92 astrocyte-specific lncRNAs are more abundantly expressed in L1, excitatory/inhibitory neuron-specific
93 lncRNAs in cortical layers (especially L2-3), and oligodendrocyte-specific lncRNAs in WM (Fig. 2E).
94 However, the majority of the subregion-specific lncRNAs are not cell-type-specific and vice versa (Fig.
95 2C, 2E), indicating a partially overlapping but independent relationship between sub-region and cell-
96 type specificity of lncRNA expression.
97
98

99 **Spatially resolved lncRNA-enriched gene modules in aged human brains**

100 We reason that lncRNAs may work with mRNAs in the same gene networks. To this end, we derived
101 pseudo-bulk matrices from each subregion as inputs and then performed co-expression network
102 analysis using the Speakeasy algorithm[16]. We generated 193 modules, with at least 30 genes per
103 module (Table S2). We then conducted module preservation (MP) analysis and revealed that cortical
104 layer modules are more preserved than those derived from WM, blood vessels, or meninges (Fig. 3B;
105 Table S3). Within each subregion, 15~60% of modules are lncRNA-enriched (Fig. 3C). For instance,
106 the cortical module 14 (L2-3_m14) contains 1,261 genes, enriched with 210 lncRNAs (Bonf. $p < 0.05$),
107 including 4 known AD-differential lncRNAs[9,10,17], 3 AD-GWAS genes[18], and 23 AD-differential lncRNA
108 genes based on our ST analysis (Fig. 3D). Gene Ontology (GO) analysis indicates that the L2-3_m14
109 module is involved in many biological processes (BP), including metabolic and cell cycle processes,
110 ncRNA processing, positive regulation of telomerase, and meiosis I (Fig. 3E, Table S4). In addition, the
111 WM module 11 (WM_m11) contains 1,148 genes, enriched with 156 lncRNAs (Bonf. $p < 0.05$), 2 of
112 which are known AD-differential lncRNAs[9,10,17], 4 are AD-GWAS genes[18] and 29 AD differential based
113 on our ST analysis (Fig. 3F). Gene Ontology (GO) analysis indicates that WM_m11 is involved in
114 carbohydrate derivative metabolism, lipid metabolic modification, and nervous system development
115 (Fig. 3G, Table S4). This result suggests that lncRNAs may exert their roles through interactions with
116 mRNAs within shared regulatory networks.
117

118 **Spatially differentially expressed (SDE) lncRNAs in postmortem AD brains**

119 To identify spatially differentially expressed (SDE) lncRNAs in postmortem AD brains, we first summed
120 the expression values of all spots within a brain section for each subregion to generate a pseudobulk
121 matrix. We then normalized the pseudobulk estimates across brain sections using TMM-voom[19] and
122 applied linear mixed models (LMM) to contrast AD against NCI individuals. We accounted for age, RNA
123 Integrity Number (RIN), postmortem interval (PMI), and batch as fixed effects and within-subject
124 correlation as a random effect. We declared significance at an α of 0.05 with false discovery rate (FDR)
125 correction for all genes (lncRNA and mRNA) and tested subregions. We found 275 SDE lncRNAs
126 (Table S5), with a greater proportion displaying negative AD association than mRNAs (Fig. 4A-B).
127 Breaking down the SDE lncRNAs by biotypes, we observed enrichment for bidirectional promoter
128 lncRNA in L3-5 and lincRNA in L6 and WM (Fig. 4C). We then compared SDE lncRNAs and mRNAs
129 from our ST analysis with those identified from bulk DLPFC RNA-seq [20] and snRNA-seq on 1,049 and
130 424 ROSMAP individuals[14], respectively. Despite only a mild overlap in AD DE genes (Fig. 4D), we
131 observed strong correlations of t-values between ST and bulk RNA-seq results for all lncRNAs (R=0.3)

132 and mRNAs (R=0.39; Fig. 4E), with the remarkable concordance for *LY86-AS1*, *FAM106A*, *LINC01007*
133 and *MIR7-3HG* (downregulated in AD), as well as *NEAT1*, *LINC00632*, *FGD5-AS1* and *LINC01094*
134 (upregulated in AD; Fig. 4E). Similarly, we also detected minimal overlapping between subregion-
135 specific and cell-type-specific AD DE lncRNAs and mRNAs (Fig. 4F). When correlating pairwise t-
136 values across subregions and cell types, we noticed a few exceptions, such as the moderate
137 correlations between L3-5 and inhibitory neurons (Fig. 4H). In addition, we also detected a DE lncRNA
138 alignment between blood vessels and microglia or oligodendrocytes (Fig. 4G), indicating shared
139 lncRNA functions in neurovascular and neuroinflammatory processes. Thus, we detected both
140 consistent and divergent results of AD DE lncRNAs between ST data and other data sets, highlighting
141 the need to explore lncRNA expressions in a range of data layers to capture their potential context-
142 specific roles or responses.
143
144 Among AD SDE lncRNAs detected in our study, a greater proportion is subregion-specific (Fig. 5A).
145 We then cross-referenced the snRNA-seq data[14] to examine whether subregion-specific lncRNA
146 expression arises from distinct cell types. However, in most cases, we did not observe a specific cell
147 type driving expression of these subregion-specific lncRNAs (Fig. 5B). On the other side, we detected
148 novel and known SDE lncRNAs[9,10,17] expressed in multiple subregions (Fig. 5C). For previously
149 reported lncRNAs[9,10,17], we also observed an alignment with our bulk RNA-seq analysis (Fig. 5C,
150 bottom panel). Interestingly, some AD SDE lncRNAs show high expression in one subregion (Fig. 2),
151 but their AD effects are predominant in other subregions. One example is *LINC00844*, which displays
152 higher expression in WM/oligodendrocytes (Fig. 2), but its AD effects are predominantly in L2-3 (Fig.
153 5B). Another is *LINC00507*, which is highly expressed in L2-3, but its AD effects are predominantly in
154 L3-6 (Fig. 5C). In addition, the X-linked gene *XIST* is among SDE lncRNAs, which prompted us to
155 examine the expression of other X-linked genes. Indeed, we found that *MECP2* and *MAOA* are
156 upregulated in AD, while *PGK1* and *HPRT1* are downregulated in AD (Fig. 5D-5F). Applying geneset
157 enrichment analysis (GSEA) to t-values of all genes for each subregion and then focusing on genesets
158 containing AD SDE lncRNAs, we found enrichments for cell motility (*MALAT1*, *SPATA13*), apoptotic
159 process (*ARMCX5-GPRASP2*), chromatin organization (*XIST*, *KCNQ1OT1*) and regulation of defense
160 response (*NEAT1*) (Fig. 5G). Notably, we also detected an enrichment of the "HDAC3 targets dn"
161 geneset that contains 3 AD SDE lncRNAs (*FGD5-AS1*, *NNT-AS1*, and *OIP5-AS1*) (Fig. 5G). In addition,
162 we found that *HDAC1*, *HDAC3*, *HDAC6*, *HDAC7*, and *HDAC10* are spatially differentially expressed in
163 AD brains (Fig. 5H). This finding echoes the accumulated studies showing HDACs' involvement in the
164 AD pathological process[21,22], suggesting a possible functional link between specific lncRNAs and
165 HDAC activity.
166

167 **Statistically inferred interaction between *OIP5-AS1* and HDAC11 is associated with AD**
168 **phenotypes**

169 HDAC inhibition has been actively investigated as a potential therapeutic approach in AD[21,23–25].
170 However, HDAC inhibitors also face challenges due to a lack of selectivity, which often results in
171 unintended off-target effects[26,27]. Our GESA results (Fig. 5D) indicate that HDACs could interact with
172 specific lncRNAs (*FGD5-AS1*, *NNT-AS1*, and *OIP5-AS1*), providing a possible solution for selectively
173 modulating HDAC activity in AD treatment. Among those three lncRNAs, *OIP5-AS1* (*Cyrano*) has been
174 implicated in many developmental processes[28–30], in the onset and progression of various cancers [31,34],
175 and recently in cerebral ischemia-reperfusion injury[35]. Thus, we decided to follow up on *OIP5-AS1* to
176 examine 1) whether genetic variation affects OIP5 AS1 expression and 2) whether OIP5 AS 1 may
177 interact with HDACs and, if so, to what extent the interaction correlates with AD clinical and pathological
178 traits.

179 We curated a set of expression quantitative trait loci (eQTLs) within 1Mb from the transcription starting
180 site (TSS) of *OIP5-AS1* for each brain cell type (Fig. 6A) from the published snRNA-seq dataset[14] and
181 applied multivariate fine-mapping [36]. Based on the posterior probability of each SNP being causal, we
182 found rs1655558 a potential causal variant influencing OIP*5-AS1* expression in multiple cell types,
183 including excitatory neurons, astrocytes, and oligodendrocytes (Fig. 6A). We then investigated the
184 interactions between *OIP5-AS1* expression levels in six major brain cell types and HDAC protein
185 abundance in the DLPFC by incorporating published proteomics data [37]. We associated the interaction
186 between cell-type-specific *OIP5-AS1* expression levels and HDAC protein abundance with three
187 categories of AD traits, i.e., cognitive decline, amyloid plaques, and tau tangles (Fig. 6B). We
188 discovered interaction effects for tau tangles and amyloid plaques, but not cognitive decline (Fig. 6C).
189 Importantly, some interactions show stronger associations with AD traits than the HDAC main effect
190 (more than an order of magnitude lower in p-value, non-circled colored dots in Fig. 6D, 6G), suggesting
191 the interaction with *OIP5-AS1* an essential element for HDACs to impact tangles and amyloid plaques.
192 We repeated this analysis with cell-type-specific HDAC mRNA expression and observed a similar trend
193 in which some interactions show stronger AD associations than main effects, but association strength
194 is lower than its protein counterpart (Fig. 6C; Fig. S1). This finding indicates that *OIP5-AS1* may interact
195 with HDAC proteins rather than mRNAs in affecting AD pathophysiology.

196 To narrow down which HDAC protein(s) interact with *OIP5 AS1* and in which cell type(s), we adjusted
197 the number of cell types and HDACs in our statistical modeling and found that *OIP5-AS1*xHDAC11
198 interaction but not the main effect of HDAC11, is associated with tau pathology in excitatory neurons
199 (Fig. 6D). Notably, the interaction effect is most strongly associated with tangle measurements of

200 hippocampus and medial temporal lobe (Fig 6E). Given that tau pathology typically progresses from
201 the hippocampus and medial temporal lobe to other cortical areas, our result indicates that the *OIP5-*
202 *AS1*xHDAC11 interaction may play a central role in tau progression and early hippocampal
203 vulnerability. Indeed, when we stratified the 424 ROSMAP individuals in the snRNA-seq data[14] into
204 three groups based on *OIP5-AS1* expression in excitatory neurons, we found that tau tangles are only
205 positively associated with HDAC11 protein level within the *OIP5-AS1*-high group (Fig. 6F).

206 The OIP5-AS1xHDAC11 interaction effect was also detected for amyloid plaques but in microglia, not
207 excitatory neurons (Fig. 6G). Similarly, the OIP5-AS1xHDAC11 interaction is strongly associated with
208 plaque measurements in the hippocampus and mesial temporal lobe (Fig. 6H). Stratifying the 424
209 ROSMAP individuals into three groups based on *OIP5-AS1* expression in microglia, we observed that
210 amyloid plaques are only positively associated with HDAC11 protein abundance within the OIP5 *AS1-*
211 low group (Fig. 6I). Overall, our analysis infers that *OIP5-AS1* interacts with HDACs, especially
212 HDAC11, in a cell-type-specific manner in contributing to AD pathophysiology.

213 **Discussion**

214 Recent advancements in sequencing technologies have revealed that a large fraction of the
215 mammalian genome is transcribed into lncRNAs[1]. Despite studies showing that brains express more
216 tissue-specific lncRNAs than most other tissue types[38,39], little is known about the spatial and cellular
217 context of lncRNAs in the human brain. We mapped the spatial expression of 7,634 lncRNAs in aged
218 human brains. Overall, we detected lower expression levels and more restricted spatial expression
219 patterns of lncRNAs than mRNAs (Fig. 1). By cross-referencing published snRNA-seq data, we detect
220 that some lncRNAs exhibit both sub-regional and cell-type specificity while others are uniquely
221 restricted to a particular brain subregion or specific cell type (Fig. 2). This partially overlapping but
222 independent pattern between sub-region and cell-type specificity of lncRNA expression indicates that
223 lncRNAs may have dual roles, operating within precise spatial regions to support localized functions
224 while also being tailored to the needs of individual cell types. Indeed, we detected many subregion-
225 specific lncRNA-enriched gene modules (Fig. 3), supporting their nuanced roles in complex regulatory
226 networks that involve cross-talks between different cell types.

227 Comparing the spatial expression of AD SDE lncRNAs to mRNAs, we also observed that lncRNAs are
228 generally more subregion-specific than mRNAs, with 115 out of 275 AD SDE lncRNAs showing
229 differential expression specifically in one subregion of the cortex. At least 13 of the AD SDE lncRNAs
230 detected in our study have been previously reported in AD studies (Fig. 5C, Table S5). For instance,
231 we detected higher expression of *MALAT1*, *NEAT1*, *BACE1-AS*, and *BDNF-AS* in AD individuals, which

is in line with extensive literature supporting their roles in AD pathogenesis through different pathways. *BACE1-AS* is reported to promote amyloid production[40–42], whereas *BDNF-AS* modulates synaptic plasticity by interacting with their mRNA counterparts[43–45]. As the major organizers of nuclear speckles and paraspeckles, *MALAT1* suppresses neuronal apoptosis and inflammation by modulating *miR-125b* expression[46,47], whereas *NEAT1* regulates tau phosphorylation and Aβ metabolism through interacting with *miR-124* and *miR-107* and histone acetyltransferases[48,49]. Furthermore, our analysis detected emerging immune- and aging-associated lncRNAs, such as *LY86-AS1*[50], *FAM106A*[51], and *MIR7-3HG*[52].

Increased *XIST* levels have been previously reported in the brains of female AD patients linked to X Chromosome Interaction (XCI), an important factor contributing to female-specific vulnerability in AD[53,54]. We detected an upregulation of *XIST* in AD, primarily in the upper cortical layers (Fig. 5C, 5D). Given that we conducted our study in only females, this upregulation of *XIST* in AD females indicates that the XCI process is disrupted in AD, which may lead to silencing of some X-linked genes or/and overexpression of other genes that escape XCI. Indeed, we detected altered expression of X-linked genes such as *MAOA, MECP2, PGK1,* and *HPRT1*(Fig. 5D, 5E), which have been reported to be essential for neuronal function, epigenetic regulations, and cellular metabolism [55–59].

Our gene set enrichment analysis shows that AD SDE lncRNAs are involved in diverse gene regulation processes, including epigenetic regulation, chromatin remodeling, RNA metabolism, synaptic signaling, and cell apoptosis. One of the mechanistic insights from this analysis is the enrichment of HDAC targets, including *FGD5-AS1*, *NNT-AS1*, and *OIP5-AS1*. HDAC pathways have been widely implicated in AD pathogenesis. Among the HDAC targets, *OIP5-AS1* is particularly interesting due to its diverse regulatory roles in cell biology[60]. First, *OIP5-AS1* has been shown to play a crucial role in cancer by regulating cell proliferation, apoptosis, migration, and invasion, primarily through its ability to sponge miRNAs and interact with chromatin modifiers such as HDACs[31–34,61]. Second, *OIP5-AS1* is upregulated in M2 microglia-derived exosomes, which inhibits neuronal pyroptosis through ubiquitination of its binding protein TXNIP[35]. Third, *OIP5-AS1* acts as a central player of a non-coding RNA network to destroy mature miR-7 and regulate neuronal activity[62]. Using statistical modeling, we inferred that the interaction between *OIP5-AS1* and HDAC proteins, especially HDAC11, is associated with tau tangles in excitatory neurons and plaque burden in microglia (Fig. 6D-I). These results indicate that *OIP5-AS1* may be involved in epigenetic regulations in AD through its interaction with HDACs in a cell-type-specific and context-dependent manner.

Limitations

This study has several data-intrinsic limitations: 1) Our ST samples were collected from aged control and AD female individuals. Therefore, whether our results can generalize to younger age groups or males remains to be determined; 2) Since the 10X Visium platform captures RNA through a polyadenylated (poly(A)) approach, our study misses non-polyadenylated lncRNAs, as well as any lncRNAs with alternative 3' end processing or shorter poly(A) tails; 3) the Visium platform is at the 55-µm resolution, limiting us from analyzing cell-type specific lncRNA expression in the spatial context; 4) the sample size of this study is relatively small, so we are likely underpowered to detect all AD DE lncRNAs; and 5) experiments are needed to validate the functional roles of lncRNAs, such as *OIP5-AS1* in AD pathogenesis.

Conclusion and Future Directions

We report a spatial expression atlas of 7,634 lncRNA genes in aged human brains, demonstrating their relatively restricted spatial expressions. We chart subregion-specific lncRNA changes and identify hundreds of AD DE lncRNAs, including known AD-associated lncRNAs, emerging immune-associated lncRNAs, and novel lncRNAs. These findings open exciting possibilities for future studies with high-resolution spatial profiling platforms, specific enrichment techniques for lncRNAs of interest, and co-detection of protein(s) in the same section, enabling finer delineation of cell-type-specific lncRNA changes in response to different AD pathologies. Furthermore, we explore the potential interaction effects of *OIPS-AS1* and HDACs in mediating AD-associated phenotypes. With various RNA-targeting technologies, such as antisense oligonucleotides (ASOs)[63] and CRISPR-Cas13d[64,65], further functional studies on *OIPS-AS1* and other AD-associated lncRNAs will shed new insights into their potential roles in AD. Because a key limitation of HDAC inhibitors in clinical trials is their non-selective action, *OIP5-AS1* might offer a possible solution for selectively modulating HDAC activity and stratifying patients for precision medicine.

Acknowledgments

We are grateful to those who agreed to donate their brains for research. We thank all the employees at RADC for their support and assistance. This study was supported by NIA grants R01AG074082 and R01AG079223 (to Y.W.), P30AG10161, P30AG72975, R01AG015819, R01AG017917, and U01AG61356 (to D. A. B.), and R01AG061798 (to C.G.).

Author contributions

B.N, D.R.A. K.L. S.T. R.V., and A.I. performed data analysis. S.D.T. and D.R.A. conducted ST experiments. J.X. performed ST data processing. M. F., V. M., and P.L.D. provided snRNA-seq data.

296 B.N., D.R.A., K.L., and Y.W. wrote the manuscript. D.A.B runs the parent ROSMAP study. Y.W.
297 conceived and supervised this study. All authors reviewed and approved the final manuscript.

298 **Lead Contact**

299 Further information and requests may be directed to the corresponding author Yanling Wang
300 (Yanling_Wang@rush.edu)

301 **Materials Availability**

302 This study did not generate new unique reagents.
303
304 **Online Methods**

305 **Tissue collection for Spatial Transcriptomics**

306 The human brain tissues were obtained through the ROSMAP (Religious Orders Study and Memory
307 and Aging Project) cohort studies at the Rush Alzheimer's Disease Center, Rush University Medical
308 Center, Chicago, IL. Written informed consent was given by the donors for brain autopsy and for the
309 use of material and clinical data for research purposes, in compliance with national ethical guidelines.
310 We selected 13 individuals clinically diagnosed as AD with high pathology and 8 controls with no
311 cognitive impairment (NCI) and no or very little pathology. All individuals are female and matched for
312 age. We chose all female individuals because there were insufficient males in the ROSMAP cohort
313 matching our selection criteria (e.g., RIN > 5, age-matched, minimal freezing artifacts in frozen
314 DLPFC). Frozen brain blocks of the right-hemisphere DLPFC from 21 individuals were cut (~ 1 cm^3),
315 transferred on dry ice, and stored at -80C.
316
317 Frozen brain blocks were embedded in OCT and cryosectioned coronally to a thickness of 10 µm
318 using a Leica CM1950 cryostat set at -17C. Sectioning was done in sets of three (middle section for
319 ST and two adjacent sections for IF), with 10-50 µm between each set. Sections were attached to
320 Visium slides and stored at -80C in a slide mailer for up to one week before proceeding with spatial
321 transcriptomics. ST-adjacent sections were attached to pre-labeled Leica superfrost plus slides and
322 stored at -80C in slide mailers for up to two weeks before proceeding with immunohistochemistry.
323

324 **Spatial Transcriptomics**

325 Spatial Transcriptomics was performed according to the Visium Spatial Gene Expression User Guide
326 (10X Genomics; CG000239). Briefly, cryosectioned tissue on Visium slides was transferred from -80C
327 to the lab on dry ice and quickly thawed for 1 min on a heat block at 37C, then immediately
328 transferred to methanol pre-equilibrated to -20C and fixed at -20C for 30 min. Sections were then
329 stained with hematoxylin and eosin, and brightfield images were acquired with a Nikon Ti2 with NIS-
330 Elements AR 5.11.01 64-bit software. After imaging, tissues were immediately permeabilized in 0.1%
331 pepsin diluted in 0.1 M HCl for 18 min at 37C. Reverse transcription, second-strand synthesis, cDNA
332 amplification (15 cycles), and library construction were performed according to the manufacturer's
333 instructions. For the first four individuals (#2, 8, 12, and 18), protocol version 'Rev A' was followed,
334 and the sample index PCR was 12 cycles. For the remaining samples, protocol version 'Rev D' was

335 followed, and the sample index PCR was 13-14 cycles. Library concentration was quantified by Qubit
336 1x dsDNA HS using a SpectraMax M3 plate reader. Library concentration and size distribution were
337 assessed by Fragment Analyzer (Agilent). Sequencing was performed in three batches on an Illumina
338 NovaSeq, targeting a minimum of 50,000 raw reads per spot.
339
340 **Spatial transcriptomics sequencing data processing**
341
342 Sequencing data were pre-processed with Space Ranger pipeline (10x Genomics), which mapped
343 the barcodes against the human genome (Gencode 27), generated FASTQ files, and generated a
344 count matrix for each section. The individual files were then merged in a Seurat object (Seurat v4.2.0)
345 and were processed in R. We calculated per-spot quality metrics and spots with low-measured genes
346 (< 500) were removed. The Seurat::SCTransform function was used to normalize and scale the UMI
347 counts based on regularized negative binomial regression. Principal component analysis (PCA) was
348 performed on the top 3000 variable genes. Using the top 50 PCs (Supplementary Fig. 1Fig. S1D) and
349 accounting for technical and biological covariates such as age, RNA integrity number (RIN), library
350 batch, and donor, we integrated the datasets using the Harmony package (v0.1.0). We explored
351 various tools for data integration and chose Harmony for its high performance, usability, and scalability.
352 We only used Harmony integration to identify clusters corresponding to brain regions. All downstream
353 analyses (differential gene expression, cell proportion estimates, and ligand-receptor analysis) were
354 performed on pre-integration count data. After visualizing the standard deviation attributed to each
355 Harmony embedding as an elbow plot (Supplementary Fig. 1Fig. S1E), we decided to use the top 10
356 Harmony embeddings. We applied Seurat::runUMAP to compute UMAP (uniform manifold
357 approximation and projection) dimension reduction and Seurat::findNeighbors and
358 Seurat::findClusters to identify clusters based on a shared nearest neighbor (SNN) clustering
359 algorithm (Louvain clustering with resolution set to 0.3; all other parameters default). This resulted in
360 11 clusters, which were annotated based on their canonical markers and spatialLIBD (v7.5) to the
361 closest anatomical cortical layer (L1, L2-3, L3-5, L5, L6), white matter (WM), meninges, and specific
362 cellular subpopulations, namely cells with high expression of hemoglobin genes ('Blood Vessel') and
363 SST/NPY ('Interneuron'). The last identified cluster, which carried a glial signature, had very few spots
364 and so was not included in downstream analyses.

365 **Co-expression network analysis in spatial transcriptomics**

366 The modules of co-expressed genes were derived using the Speakeasy (SE) algorithm v1, Matlab
367 version[16] . We created pseudo-bulk gene expression by summing the counts per donor, then splitting
368 by UMAP cluster. Lowly expressed genes (less than 1 count per million, CPM) were removed, and
369 the variancePartition R function was applied to capture the major sources of variation, as previously
370 described [15]. The input for SE consisted of the residuals after normalization using tmm.voom and
371 adjustment for library batch, RIN, age, and PMI. We built the modules separately for each UMAP
372 cluster, using the results from 100 initializations of SE and Spearman correlation. This resulted in 193
373 modules, each with at least 30 genes (L1 = 30, L2-3 = 21, L3-5 = 20, L5 = 20, L6 = 20, Meninges =
374 33, WM = 20, and blood vessels = 29). The module assignments are provided in Table S2.
375
376 *Functional Enrichment Analysis (FEA)*

Each module was annotated using the gprofiler software (v2_0.2.1) via the g:GOSt R function [66]. This tool maps genes to functional information sources and detects statistically significantly enriched terms. These sources include the GO database, pathways from KEGG, Reactome, and WikiPathways, miRNA targets from miRTarBase, regulatory motif matches from TRANSFAC, tissue specificity from the Human Protein Atlas, protein complexes from CORUM, and human disease phenotypes from the Human Phenotype Ontology. For multiple testing correction, we used the default g:SCS method unless otherwise specified. The FEA results are available in Table S4.

Module Preservation (MP) Analysis

To assess whether the modules were preserved across distinct UMAP clusters, we used the MP function from the WGCNA R package (v1.70-3)[67]. Pairwise comparisons were performed for all 193 modules. We then estimated the mean and variance of the preservation statistic under the null hypothesis that there is no relationship between module assignments in the reference and test datasets. Fifteen distinct preservation statistics were calculated (e.g., module density, mean expression, connectivity), each standardized by its mean and variance to define a Z statistic for each preservation measure. Under these assumptions, each Z statistic follows a normal distribution if the module is not preserved. To compare preservation across modules, we calculated a composite preservation measure using the following equation:

$$Zsummary = \frac{Zdensity + Zconnectivity}{2}$$

Modules with Z < 2 were considered not preserved, those with Z between 2 and 10 were considered preserved, and modules with Z > 10 were considered highly preserved. Zsummary stats are available in Table S3.

Statistical analysis to identify AD-differential genes

For each brain section of a subject, we summed the UMI counts of all spots belonging to a subregion to generate a pseudobulk estimate for each gene. We only kept expressed genes with counts per million (CPM) > 1 in at least 80% of the brain sections. With the pseudobulk estimates, we estimated the library sizes of the brain sections using the trimmed mean of M-values (TMM) of edgeR[68] (edgeR_3.36.0) and transformed the pseudobulk estimates into $\log_2$ CPM using voom-limma (limma_3.50.1). For each subregion, we excluded brain sections with <50 spots. To contrast the normalized pseudobulk expression between AD and controls, we applied linear mixed models (LMM), accounting for age, PMI, RIN, and batch as fixed effects and modeled within-subject correlation with a random effect. We declared significance at an α of 0.05 with false discovery rate (FDR) correction across all genes and all subregions.

For interpretation, we applied GSEA[69] with AD differential t-values of each subregion as scores, and GO terms and canonical pathways as genesets. To characterize lncRNAs with respect to brain cell types, we used the pseudobulk expression data from a published snRNAseq dataset of 424 ROSMAP individuals [14]. For each of the major cell types, we contrasted pseudobulk expression of AD subjects vs. controls using multiple regression, accounting for age, PMI, RIN, and batch. For further

comparison, we repeated this AD differential expression analysis with bulk DLPFC RNA-seq data from 1049 individuals[20].

References

1. Mattick, J. S. *et al.* Long non-coding RNAs: definitions, functions, challenges and recommendations. *Nat. Rev. Mol. Cell Biol.* **24**, 430–447 (2023).
2. Statello, L., Guo, C.-J., Chen, L.-L. & Huarte, M. Gene regulation by long non-coding RNAs and its biological functions. *Nat. Rev. Mol. Cell Biol.* **22**, 96–118 (2020).
3. Wang, K. C. & Chang, H. Y. Molecular mechanisms of long noncoding RNAs. *Mol. Cell* **43**, 904–914 (2011).
4. Guttman, M. *et al.* Chromatin signature reveals over a thousand highly conserved large non-coding RNAs in mammals. *Nature* **458**, 223–227 (2009).
5. Kung, J. T. Y., Colognori, D. & Lee, J. T. Long noncoding RNAs: past, present, and future. *Genetics* **193**, 651–669 (2013).
6. Djebali, S. *et al.* Landscape of transcription in human cells. *Nature* **489**, 101–108 (2012).
7. Cabili, M. N. *et al.* Integrative annotation of human large intergenic noncoding RNAs reveals global properties and specific subclasses. *Genes Dev.* **25**, 1915–1927 (2011).
8. Derrien, T. *et al.* The GENCODE v7 catalog of human long noncoding RNAs: analysis of their gene structure, evolution, and expression. *Genome Res.* **22**, 1775–1789 (2012).
9. Wu, X., Xia, P., Yang, L., Lu, C. & Lu, Z. The roles of long non-coding RNAs in Alzheimer's disease diagnosis, treatment, and their involvement in Alzheimer's disease immune responses. *Noncoding RNA Res.* **9**, 659–666 (2024).
10. Policarpo, R. & d'Ydewalle, C. Missing lnc(RNAs) in Alzheimer's Disease? *Genes* **13**, (2021).
11. Lan, Z., Chen, Y., Jin, J., Xu, Y. & Zhu, X. Long non-coding RNA: Insight into mechanisms of Alzheimer's disease. *Front. Mol. Neurosci.* **14**, 821002 (2021).
12. Huang, Z., Zhao, J., Wang, W., Zhou, J. & Zhang, J. Depletion of LncRNA NEAT1 rescues mitochondrial dysfunction through NEDD4L-dependent PINK1 degradation in animal models of Alzheimer's disease. *Front. Cell. Neurosci.* **14**, 28 (2020).
13. Riva, P., Ratti, A. & Venturin, M. The Long Non-Coding RNAs in Neurodegenerative Diseases: Novel Mechanisms of Pathogenesis. *Curr. Alzheimer Res.* **13**, 1219–1231 (2016).
14. Fujita, M. *et al.* Cell subtype-specific effects of genetic variation in the Alzheimer's disease brain. *Nat. Genet.* **56**, 605–614 (2024).
15. Avey, D. R. *et al.* Uncovering plaque-Glia niches in human Alzheimer's Disease brains using spatial transcriptomics. *bioRxivorg* (2024) doi:10.1101/2024.09.05.611566.
16. Gaiteri, C. *et al.* Identifying robust communities and multi-community nodes by combining top-down and bottom-up approaches to clustering. *Sci. Rep.* **5**, 1–14 (2015).
17. Li, D. *et al.* Insights into lncRNAs in Alzheimer's disease mechanisms. *RNA Biol.* **18**, 1037–1047 (2021).
18. Bellenguez, C. *et al.* New insights into the genetic etiology of Alzheimer's disease and related dementias. *Nat. Genet.* **54**, 412–436 (2022).
19. Law, C. W., Chen, Y., Shi, W. & Smyth, G. K. voom: Precision weights unlock linear model analysis tools for RNA-seq read counts. *Genome Biol.* **15**, R29 (2014).
20. Mostafavi, S. *et al.* A molecular network of the aging human brain provides insights into the pathology and cognitive decline of Alzheimer's disease. *Nat. Neurosci.* **21**, 811–819 (2018).

21. Shukla, S. & Tekwani, B. L. Histone deacetylases inhibitors in neurodegenerative diseases, neuroprotection and neuronal differentiation. *Front. Pharmacol.* **11**, 537 (2020).
22. Govindarajan, N. *et al.* Reducing HDAC6 ameliorates cognitive deficits in a mouse model for Alzheimer's disease. *EMBO Mol. Med.* **5**, 52–63 (2013).
23. Onishi, T. *et al.* A novel orally active HDAC6 inhibitor T-518 shows a therapeutic potential for Alzheimer's disease and tauopathy in mice. *Sci. Rep.* **11**, 15423 (2021).
24. Yang, S.-S., Zhang, R., Wang, G. & Zhang, Y.-F. The development prospection of HDAC inhibitors as a potential therapeutic direction in Alzheimer's disease. *Transl. Neurodegener.* **6**, 19 (2017).
25. Zhang, M. *et al.* Histone deacetylase inhibitors VPA and WT161 ameliorate the pathological features and cognitive impairments of the APP/PS1 Alzheimer's disease mouse model by regulating the expression of APP secretases. *Alzheimers. Res. Ther.* **16**, 15 (2024).
26. Kumar, V., Kundu, S., Singh, A. & Singh, S. Understanding the role of histone deacetylase and their inhibitors in neurodegenerative disorders: Current targets and future perspective. *Curr. Neuropharmacol.* **20**, 158–178 (2022).
27. Ru, J. *et al.* Technologies of targeting histone deacetylase in drug discovery: Current progress and emerging prospects. *Eur. J. Med. Chem.* **261**, 115800 (2023).
28. Yang, J.-H. *et al.* LncRNA OIP5-AS1-directed miR-7 degradation promotes MYMX production during human myogenesis. *Nucleic Acids Res.* **50**, 7115–7133 (2022).
29. Zhuang, A. *et al.* Loss of the long non-coding RNA OIP5-AS1 exacerbates heart failure in a sex-specific manner. *iScience* **24**, 102537 (2021).
30. Hunkler, H. J. *et al.* The long non-coding RNA Cyrano is dispensable for pluripotency of Murine and human pluripotent stem cells. *Stem Cell Reports* **15**, 13–21 (2020).
31. Kotake, Y., Matsunaga, N., Wakasaki, T. & Okada, R. OIP5-AS1 promotes proliferation of non-small-cell lung cancer and head and neck squamous cell carcinoma cells. *Cancer Genomics Proteomics* **18**, 543–548 (2021).
32. Wu, L., Liu, Y., Guo, C. & Shao, Y. LncRNA OIP5-AS1 promotes the malignancy of pancreatic ductal adenocarcinoma via regulating miR-429/FOXD1/ERK pathway. *Cancer Cell Int.* **20**, 296 (2020).
33. Arunkumar, G. *et al.* LncRNA OIP5-AS1 is overexpressed in undifferentiated oral tumors and integrated analysis identifies as a downstream effector of stemness-associated transcription factors. *Sci. Rep.* **8**, 7018 (2018).
34. Gong, M. *et al.* OIP5 is a novel prognostic biomarker in clear cell renal cell cancer correlating with immune infiltrates. *Front. Immunol.* **13**, 805552 (2022).
35. Li, Z. *et al.* Exosomal OIP5-AS1 attenuates cerebral ischemia-reperfusion injury by negatively regulating TXNIP protein stability and inhibiting neuronal pyroptosis. *Int. Immunopharmacol.* **127**, 111310 (2024).
36. Zou, Y., Carbonetto, P., Xie, D., Wang, G. & Stephens, M. Fast and flexible joint fine-mapping of multiple traits via the Sum of Single Effects model. *bioRxivorg* (2024) doi:10.1101/2023.04.14.536893.
37. Johnson, E. C. B. *et al.* Large-scale deep multi-layer analysis of Alzheimer's disease brain reveals strong proteomic disease-related changes not observed at the RNA level. *Nat. Neurosci.* **25**, 213–225 (2022).
38. Jiang, C. *et al.* Identifying and functionally characterizing tissue-specific and ubiquitously expressed human lncRNAs. *Oncotarget* **7**, 7120–7133 (2016).

39. de Goede, O. M. *et al.* Population-scale tissue transcriptomics maps long non-coding RNAs to complex disease. *Cell* **184**, 2633–2648.e19 (2021).
40. Li, F. *et al.* The effect of BACE1-AS on β-amyloid generation by regulating BACE1 mRNA expression. *BMC Mol. Biol.* **20**, 23 (2019).
41. Faghihi, M. A. *et al.* Expression of a noncoding RNA is elevated in Alzheimer's disease and drives rapid feed-forward regulation of beta-secretase. *Nat. Med.* **14**, 723–730 (2008).
42. Zhang, W., Zhao, H., Wu, Q., Xu, W. & Xia, M. Knockdown of BACE1-AS by siRNA improves memory and learning behaviors in Alzheimer's disease animal model. *Exp. Ther. Med.* **16**, 2080–2086 (2018).
43. Modarresi, F. *et al.* Inhibition of natural antisense transcripts in vivo results in gene-specific transcriptional upregulation. *Nat. Biotechnol.* **30**, 453–459 (2012).
44. Jiao, S.-S. *et al.* Brain-derived neurotrophic factor protects against tau-related neurodegeneration of Alzheimer's disease. *Transl. Psychiatry* **6**, e907 (2016).
45. Ding, Y., Luan, W., Shen, X., Wang, Z. & Cao, Y. LncRNA BDNF-AS as ceRNA regulates the miR-9-5p/BACE1 pathway affecting neurotoxicity in Alzheimer's disease. *Arch. Gerontol. Geriatr.* **99**, 104614 (2022).
46. Ma, P. *et al.* Long non-coding RNA MALAT1 inhibits neuron apoptosis and neuroinflammation while stimulates neurite outgrowth and its correlation with MiR-125b mediates PTGS2, CDK5 and FOXQ1 in Alzheimer's disease. *Curr. Alzheimer Res.* **16**, 596–612 (2019).
47. Bernard, D. *et al.* A long nuclear-retained non-coding RNA regulates synaptogenesis by modulating gene expression. *EMBO J.* **29**, 3082–3093 (2010).
48. Dong, L.-X. *et al.* LncRNA NEAT1 promotes Alzheimer's disease by down regulating micro-27a-3p. *Am. J. Transl. Res.* **13**, 8885–8896 (2021).
49. Ke, S. *et al.* Long noncoding RNA NEAT1 aggravates Aβ-induced neuronal damage by targeting miR-107 in Alzheimer's disease. *Yonsei Med. J.* **60**, 640–650 (2019).
50. Bútová, R. *et al.* LncRNAs LY86-AS1 and VIM-AS1 distinguish plasma cell leukemia patients from multiple myeloma patients. *Biomedicines* **9**, 1637 (2021).
51. Kurniansyah, N. *et al.* An integrated multi-omics analysis of sleep-disordered breathing traits implicates P2XR4 purinergic signaling. *Commun. Biol.* **6**, 125 (2023).
52. Tan, Y. *et al.* lncRNA-associated ceRNA network revealing the potential regulatory roles of ferroptosis and immune infiltration in Alzheimer's disease. *Front. Aging Neurosci.* **15**, 1105690 (2023).
53. Bajic, V. P. *et al.* The X files: 'the mystery of X chromosome instability in Alzheimer's disease'. *Front. Genet.* **10**, 1368 (2019).
54. Garcia, A. X., Xu, J., Cheng, F., Ruppin, E. & Schäffer, A. A. Altered gene expression in excitatory neurons is associated with Alzheimer's disease and its higher incidence in women. *Alzheimers Dement. (N. Y.)* **9**, e12373 (2023).
55. Sun, X. *et al.* The MAOA gene influences the neural response to psychosocial stress in the human brain. *Front. Behav. Neurosci.* **14**, 65 (2020).
56. Ziermans, T. *et al.* Working memory brain activity and capacity link MAOA polymorphism to aggressive behavior during development. *Transl. Psychiatry* **2**, e85 (2012).
57. Chua, G. N. L. *et al.* Differential dynamics specify MeCP2 function at nucleosomes and methylated DNA. *Nat. Struct. Mol. Biol.* 1–9 (2024).
58. Chu, S.-L. *et al.* Phosphoglycerate kinase 1 acts as a cargo adaptor to promote EGFR transport to the lysosome. *Nat. Commun.* **15**, 1021 (2024).

554 59. Vinokurov, A. Y. *et al.* HPRT1 deficiency induces alteration of mitochondrial energy metabolism
555 in the brain. *Mol. Neurobiol.* **60**, 3147–3157 (2023).
556 60. Wooten, S. & Smith, K. N. Long non-coding RNA OIP5-AS1 (Cyrano): A context-specific
557 regulator of normal and disease processes. *Clin. Transl. Med.* **12**, e706 (2022).
558 61. Mei, J. *et al.* OIP5-AS1 modulates epigenetic regulator HDAC7 to enhance non-small cell lung
559 cancer metastasis via miR-140-5p. *Oncol. Lett.* **20**, 7 (2020).
560 62. Kleaveland, B., Shi, C. Y., Stefano, J. & Bartel, D. P. A network of noncoding regulatory RNAs
561 acts in the mammalian brain. *Cell* **174**, 350–362.e17 (2018).
562 63. Mummery, C. J. *et al.* Tau-targeting antisense oligonucleotide MAPTRx in mild Alzheimer's
563 disease: a phase 1b, randomized, placebo-controlled trial. *Nat. Med.* **29**, 1437–1447 (2023).
564 64. Kuo, H.-C., Prupes, J., Chou, C.-W. & Finkelstein, I. J. Massively parallel profiling of RNA-
565 targeting CRISPR-Cas13d. *Nat Commun* **15**, (2024).
566 65. Wessels, H.-H. *et al.* Massively parallel Cas13 screens reveal principles for guide RNA design.
567 *Nat. Biotechnol.* **38**, 722–727 (2020).
568 66. Kolberg, L. *et al.* g:Profiler-interoperable web service for functional enrichment analysis and gene
569 identifier mapping (2023 update). *Nucleic Acids Res.* **51**, W207–W212 (2023).
570 67. Langfelder, P., Luo, R., Oldham, M. C. & Horvath, S. Is my network module preserved and
571 reproducible? *PLoS Comput. Biol.* **7**, e1001057 (2011).
572 68. Robinson, M. D., McCarthy, D. J. & Smyth, G. K. edgeR: a Bioconductor package for differential
573 expression analysis of digital gene expression data. *Bioinformatics* **26**, 139–140 (2010).
574 69. Subramanian, A. *et al.* Gene set enrichment analysis: A knowledge-based approach for
575 interpreting genome-wide expression profiles. *Proceedings of the National Academy of Sciences*
576 **102**, 15545–15550 (2005).

577
578
579
580
581
582
583
584
585
586
587
588
589
590
591
592
593
594
595
596
597

Main Figures

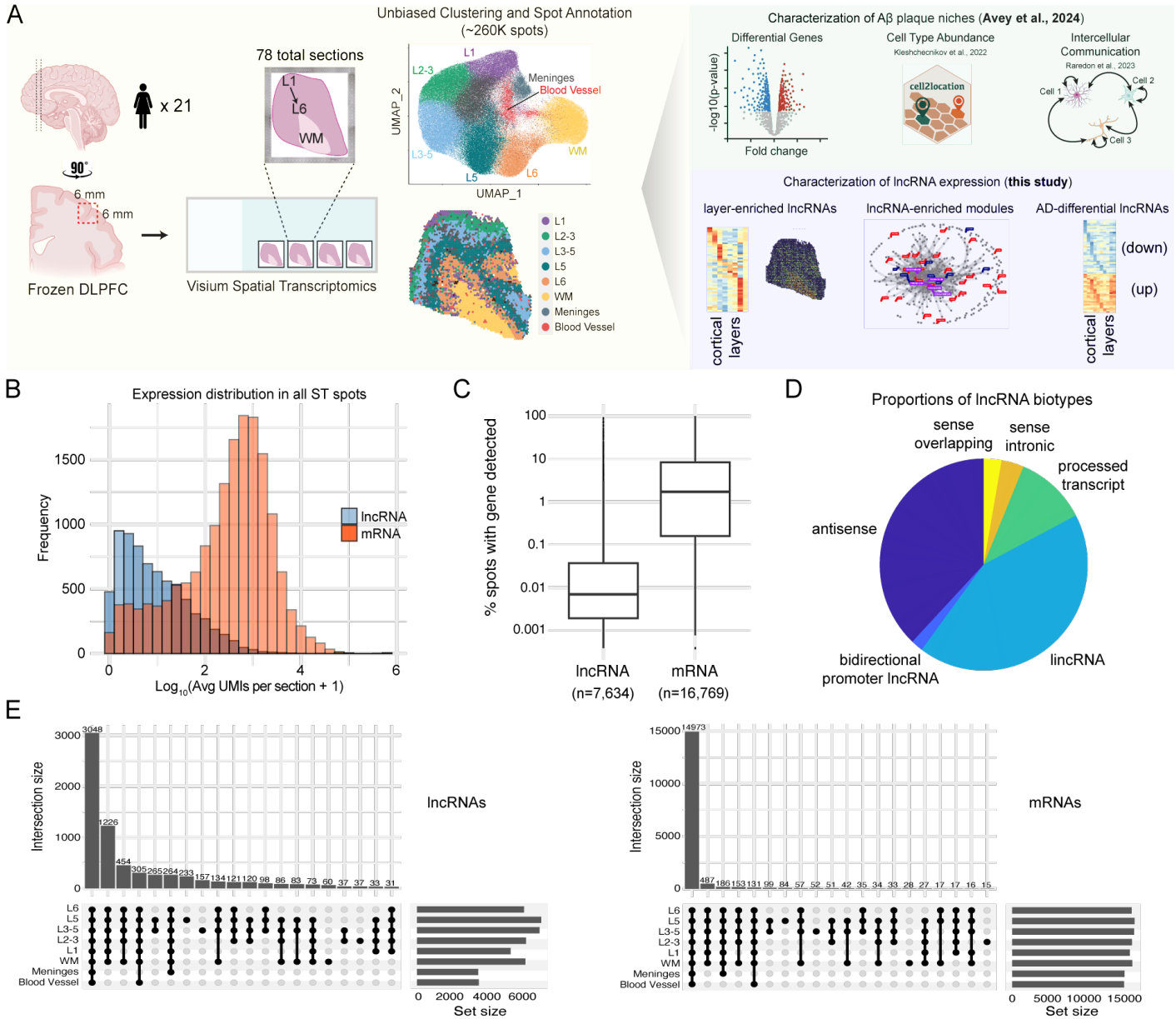

Figure 1. ST reveals the spatial expression of lncRNAs. (A) Study overview. **(B)** Comparison of the expression distributions of lncRNAs and protein-coding genes (mRNAs). **(C)** Comparison of percentage of ST spots with non-zero expression for lncRNAs and mRNAs. **(D)** Proportion of detected lncRNAs (aggregated across subregions) belonging to each biotype. **(E)** Upset plots showing the numbers of lncRNAs (left) and mRNAs (right) detected in the top 20 most common intersections of subregions.

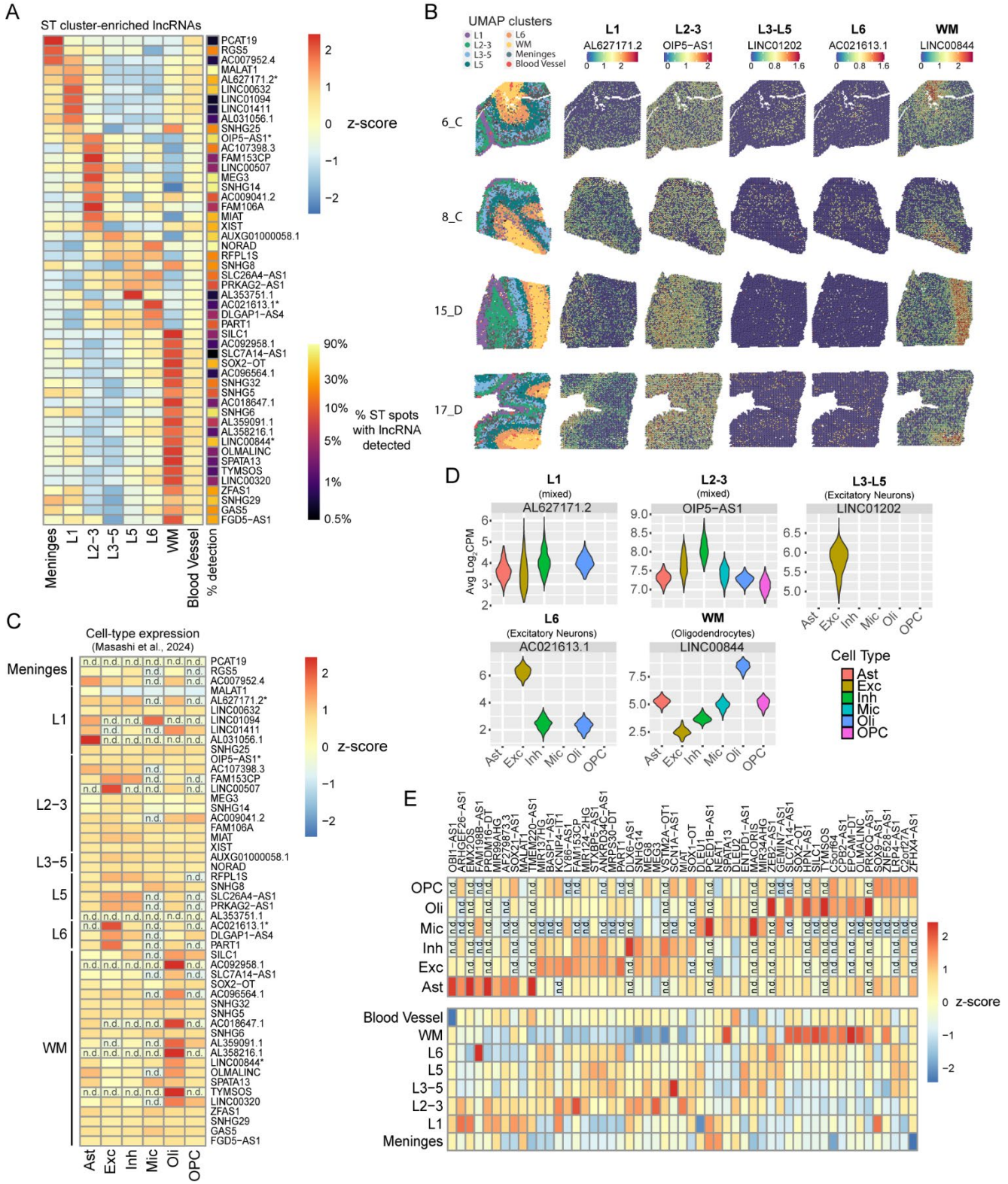

Figure 2. Identification of subregion- and cell-type-enriched lncRNAs. (A) Heatmap showing scaled expression (z-score) of the top 50 subregion-specific lncRNAs. An additional column to the right shows the percentage of spots with non-zero expression for each lncRNA (*exemplar lncRNAs shown in panel B). **(B)** UMAP and expression feature plots for 4 representative sections, showing 5 examples of lncRNAs with enriched expression in specific cortical layers or white matter (WM). **(C)** Scaled snRNA-seq expression of the same 50 subregion-specific lncRNAs shown in (A) for the 6 most abundant brain cell types (*exemplar lncRNAs shown in panel B; n.d.: not detected). **(D)** Violin plots showing expression distributions among 6 major brain cell types for the 5 lncRNAs shown in (B). **(E)** Scaled expression by cell type (top) and ST subregion (bottom) for the top 10 cell-type-specific lncRNAs from each of the 6 major brain cell types.

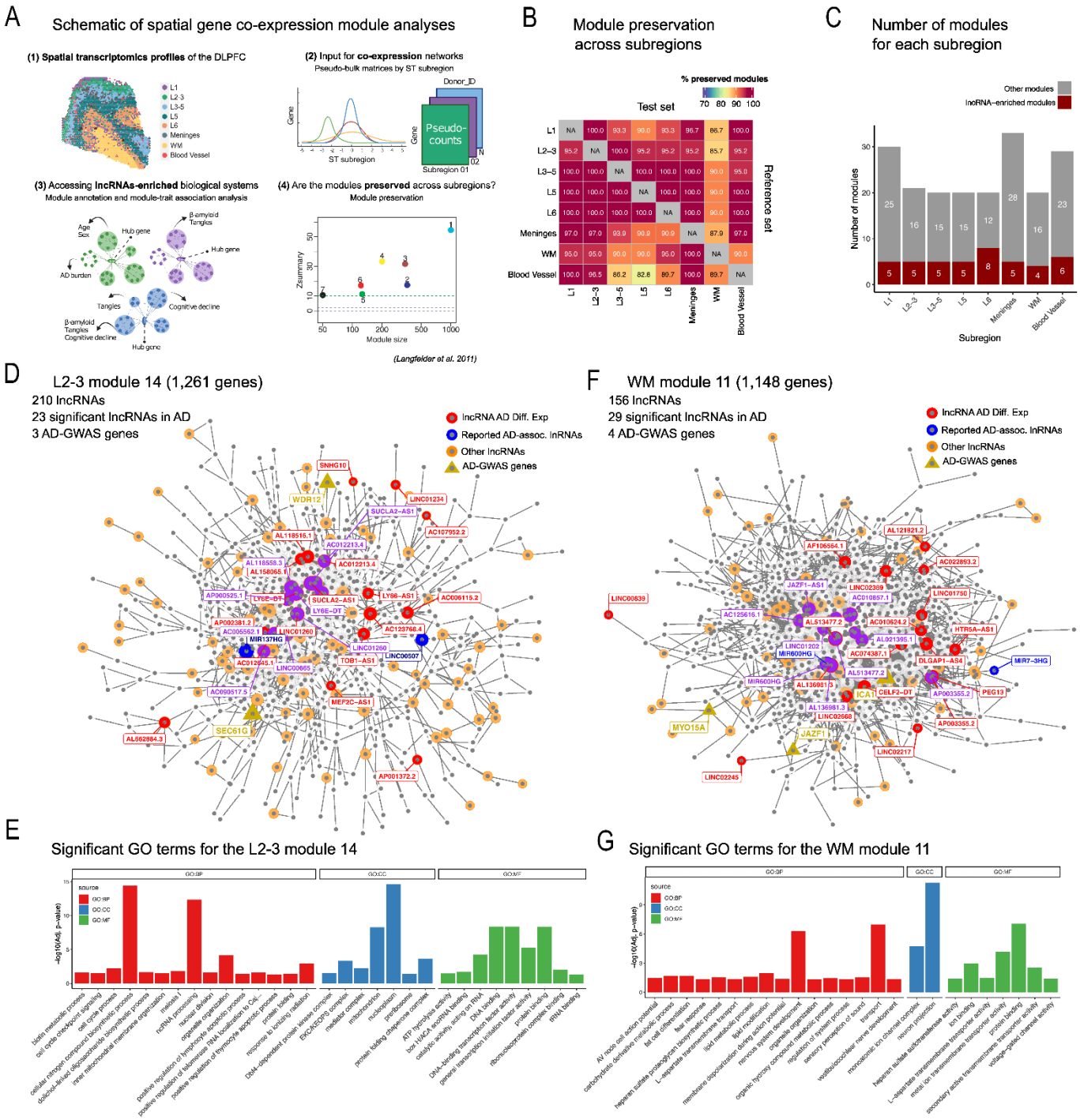

Figure 3. Subregion-specific gene modules from ST data highlight a central role for lncRNAs. **(A)** Schematic of gene expression module generation and downstream analyses. **(B)** Heatmap showing the percentage of preserved modules between each pairwise comparison of UMAP clusters. **(C)** Stacked barplot shows the number of modules in each subregion. Red colors for the lncRNA-enriched modules. **(D)** Network connectivity map for L2-3 m14, illustrating high connectivity of lncRNAs (correlation > 0.9). **(E)** Enriched Gene Ontology (GO) terms (FDR at 0.05) from functional enrichment analysis of an example lncRNA-enriched module (L2-3 m14). **(F)** Network connectivity map for WM module 11, illustrating high connectivity of lncRNAs (correlation > 0.95). **(G) Enriched** GO terms (FDR at 0.05) from functional enrichment analysis for the WM module 11. **(E, G)** The GO biological process terms were collapsed, keeping only the top GO parent functions to avoid redundancy. The y-axis and bar size represent the significance in -$\log_{10}$(Adj. p-Value). GO biological process (BP), cellular component (CC), and GO molecular function (MF).

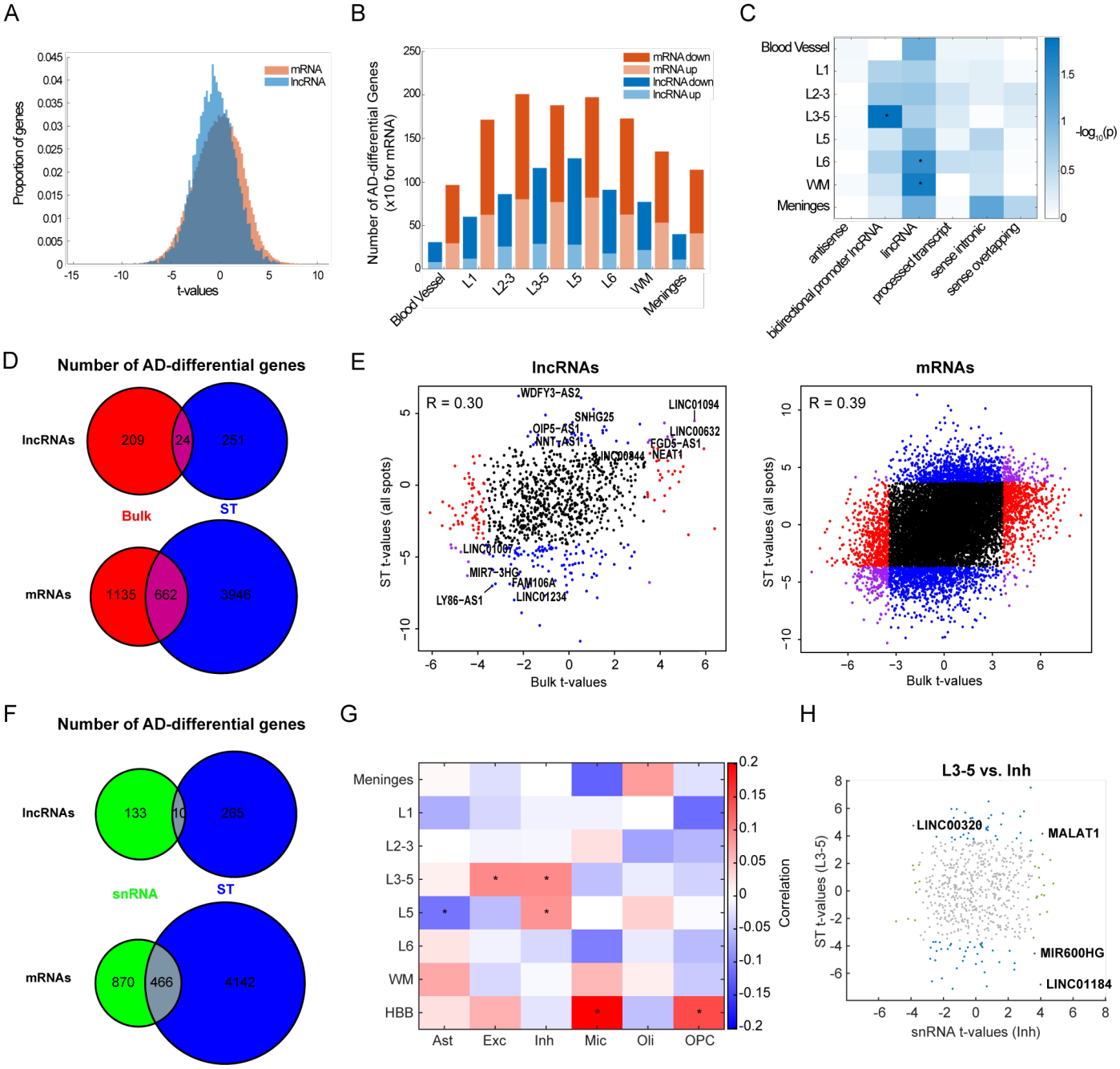

Figure 4. Contrasting AD-differential lncRNAs and mRNAs across data modalities
(A) Histogram showing the distribution of AD-differential t-values for mRNAs and lncRNAs. **(B)** Total numbers of AD-differential lncRNAs and mRNAs for each subregion. **(C)** Heatmap showing the enrichment of AD-differential lncRNAs for specific biotypes. **(D)** Overlapsin AD-differential lncRNAs and mRNAs between ST and bulk RNA-seq. **(E)** Scatterplots of ST (y-axis) vs. bulk RNA-seq (x-axis) AD-differential t-values for lncRNAs (left) and mRNAs (right). Correlation (R) value is shown at the top left of each plot. **(F)** Overlaps in AD-differential lncRNAs and mRNAs between ST and snRNA-seq. **(G)** Heatmap showing correlation (R) between subregions-cell-types based on their AD differential t-values(*p<0.05). **(H)** Scatterplot of ST L3-5 (y-axis) vs. snRNA-seq inhibitory neuron (x-axis) AD-differential t-values (restricted tolncRNAs).

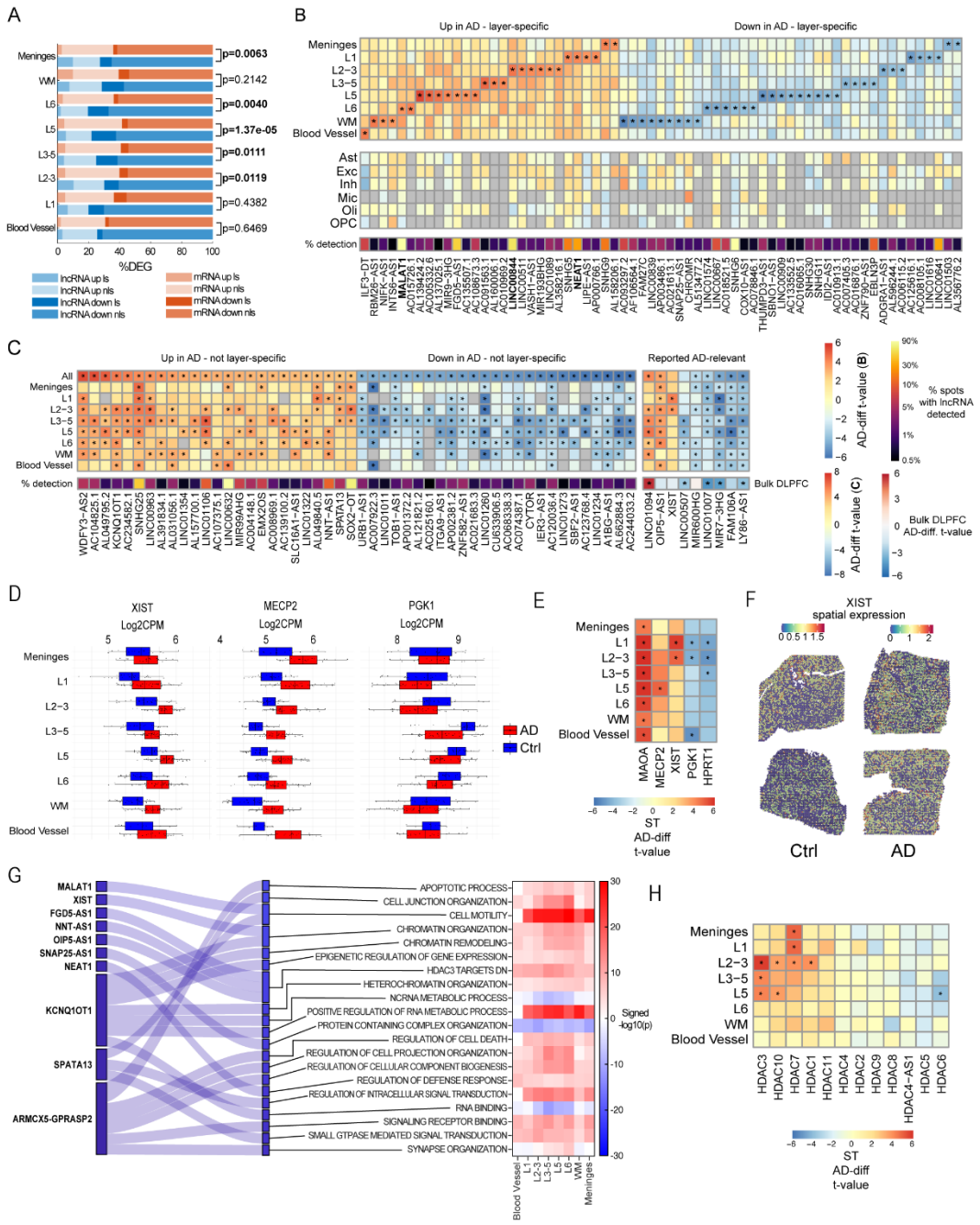

Figure 5. Characterization of AD-differential lncRNAs by ST. (A) The percentage of DEGs in each ST subregion, split by lncRNA/mRNA, up/down in AD, and whether they are subregion-specific (ss) or not (nss). Fisher's exact test was applied to assess differences in subregion-specificity between lncRNA and mRNA with p-values indicated. **(B)** (top) Heatmap showing t-values of AD-differential lncRNAs passing FDR correction specifically for one ST subregion, i.e. subregion-specific (*p<5e-4 in designated subregion and p>0.001 in all others). (bottom) AD-differential t-values for 6 brain cell types. An additional row below shows the percentage of ST spots with non-zero expression for each lncRNA. **(C)** (left) Heatmap showing t-values of AD-differential lncRNAs passing FDR correction in two or more ST subregions, i.e. not subregion-specific (*p<5e-4). An additional row below shows the percentage of ST spots with non-zero expression for each lncRNA. (right) AD-differential t-values for a subset of 13 lncRNAs with previously reported AD association, including t-values from DLPFC bulk RNA-seq below. **(D)** Boxplots of subregion-specific pseudobulk expression from ST data for XIST, MECP2, and PGK1 (X-linked genes), all of which show altered expression in AD in one or more subregions. **(E)** Heatmap showing a subset of X-linked genes with AD-differential expression in one or more subregions (*p<5e-4). **(F)** XIST spatial expression plots for two control (Ctrl) and two AD sections. **(G)** Sankey diagram and heatmap showing a subset of enriched genesets and AD differential lncRNAs belonging to those genesets. (**H**) A subset of HDAC genes display AD-differential expression in specific ST subregions (*p<5e-4).

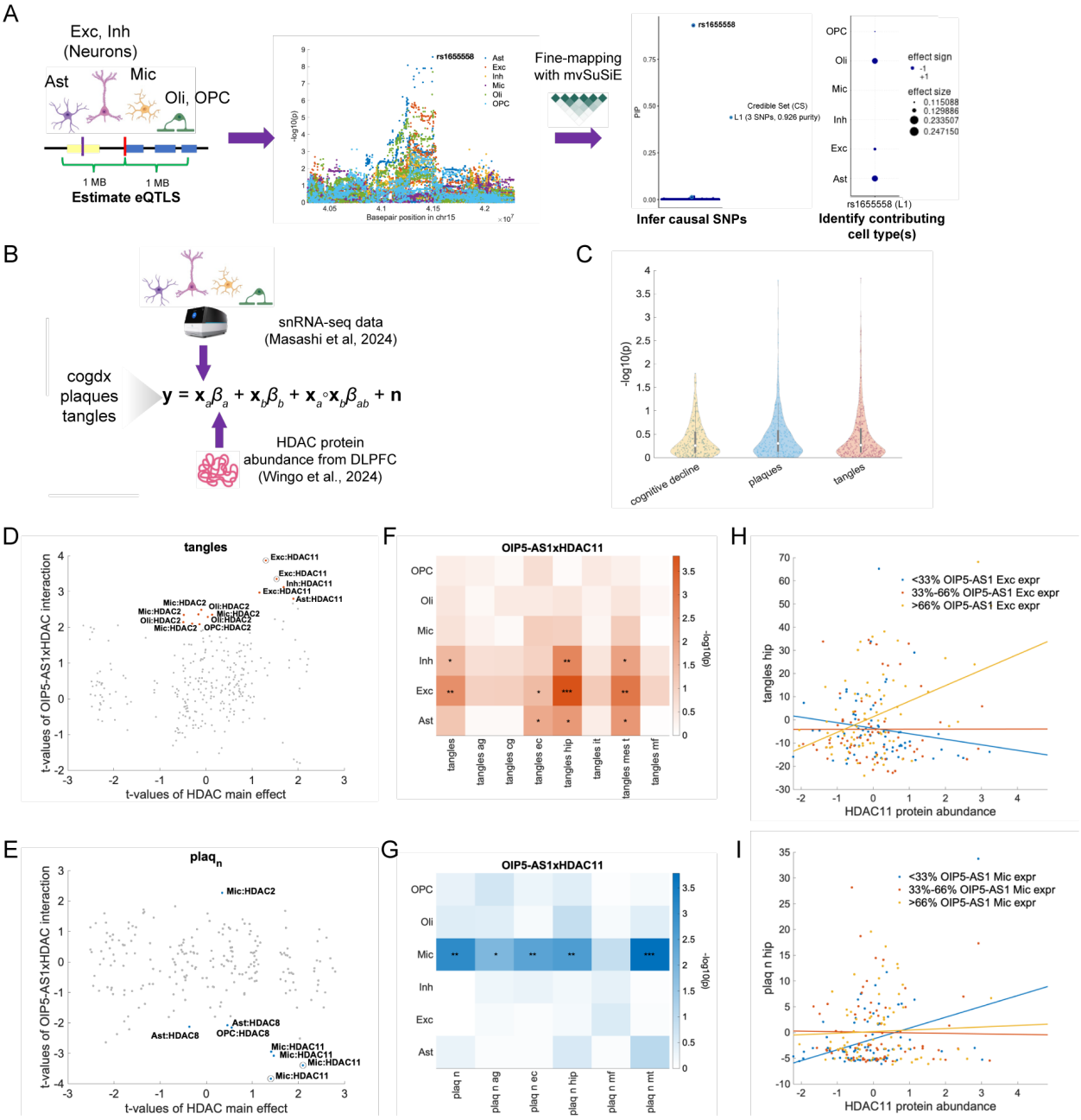

Figure 6. Genetic analysis of OIP5-AS1 and its interaction with HDAC. (A) Colocalization analysis of OIP5-AS1 eQTLs across major brain cell types. Applying mvSuSiE found rs1655558 to be a potential driver of OIP5-AS1 expression in astrocytes, oligodendrocytes, and excitatory neurons (Ast: Astrocyte, Exc: excitatory, Inh: Inhibitory, Mic: Microglia, Oli: Oligodendrocyte, OPC: Oligodendrocyte progenitor cell, PIP: posterior inclusion probability; cartoon cell type images created in BioRender.com). **(B)** Summary of OIP5-AS1xHDAC interaction analysis. snRNAseq (Masashi et al., 2024) and proteomic (Wingo et al., 2024) data from human DLPFC were used to associate the statistical interaction between OIP5-AS1 expression level (in specific cell types) and protein abundance of each of six HDACs with AD phenotypes, including cognitive decline (cogdx), amyloid plaques, and tau tangles. Cognition was assessed over multiple domains and pathologies were measured in multiple brain regions. **(C)** Each point in the violin plot represents the –log10(p) of the interaction effect of OIP5-AS1 and HDAC for a given combination of cell type, HDAC, and AD phenotype. Higher associations were observed for plaques and tangles. **(D)** Scatterplots showing t-values of the HDAC main effect (x-axis) and the OIP5-AS1xHDAC interaction for tangles measured in multiple brain regions**.** Dots are colored but not circled if interaction p<0.05 and an order of magnitude lower than the main effect p-value. Circled dots are interactions passing multiple comparison correction for the number of HDACs and cell types. OIP5-AS1xHDAC11 interaction shows the strongest association with tangles. (E) Heatmap of OIP5-AS1xHDAC11 interaction p-values across cell types and tangles in different brain regions shown (ag: anterior gyrus, ec:

entorhinal cortex, hip: hippocampus, mf: medial frontal, mt: medial temporal, cg: cingulate gyrus, it: inferior temporal, mes_t: mesial temporal). **(F)** An exemplary visualization of interaction effect. Individuals were stratified into three groups based on the expression of OIP5-AS1 in excitatory neurons. For each group, HDAC11 protein abundance was plotted against tangle level in the hippocampus. (G-I) are plaque burden counterparts of (D-F).

Supplementary Tables.

Table S1. Subregion- and cell-type-enriched lncRNAs

Table S2. ST gene expression module assignments

Table S3. ST gene expression module preservation

Table S4. ST gene expression module FEA

Table S5. Differentially expressed lncRNAs in AD (ST, bulk, snRNA)

Table S6. GSEA of ST genes

Supplementary Figures.

Figure S1. Association of lncRNA OIP5-AS1 with AD phenotypes using HDAC